Article

TRANSPARENT PROCESS OPEN ACCESS

THE EMBO JOURNAL

Rotational motion and rheotaxis of human sperm do not require functional CatSper channels and transmembrane Ca^{2+} signaling

Christian Schiffer[1], Steffen Rieger[2], Christoph Brenker[1], Samuel Young[1], Hussein Hamzeh[3], Dagmar Wachten[4,5], Frank Tüttelmann[6], Albrecht Röpke[6], U Benjamin Kaupp[3], Tao Wang[1,7], Alice Wagner[1,6], Claudia Krallmann[1], Sabine Kliesch[1], Carsten Fallnich[2,8,*] & Timo Strünker[1,8,**]

Abstract

Navigation of sperm in fluid flow, called rheotaxis, provides long-range guidance in the mammalian oviduct. The rotation of sperm around their longitudinal axis (rolling) promotes rheotaxis. Whether sperm rolling and rheotaxis require calcium (Ca^{2+}) influx via the sperm-specific Ca^{2+} channel CatSper, or rather represent passive biomechanical and hydrodynamic processes, has remained controversial. Here, we study the swimming behavior of sperm from healthy donors and from infertile patients that lack functional CatSper channels, using dark-field microscopy, optical tweezers, and microfluidics. We demonstrate that rolling and rheotaxis persist in CatSper-deficient human sperm. Furthermore, human sperm undergo rolling and rheotaxis even when Ca^{2+} influx is prevented. Finally, we show that rolling and rheotaxis also persist in mouse sperm deficient in both CatSper and flagellar Ca^{2+}-signaling domains. Our results strongly support the concept that passive biomechanical and hydrodynamic processes enable sperm rolling and rheotaxis, rather than calcium signaling mediated by CatSper or other mechanisms controlling transmembrane Ca^{2+} flux.

Keywords Ca^{2+} signaling; CatSper; rheotaxis; rolling; human sperm
Subject Categories Cell Adhesion, Polarity & Cytoskeleton; Membranes & Trafficking; Signal Transduction
DOI 10.15252/embj.2019102363 | Received 30 April 2019 | Revised 30 October 2019 | Accepted 6 December 2019 | Published online 19 January 2020
The EMBO Journal (2020) 39: e102363

Introduction

In fluid flow, mammalian sperm realign their swimming path and move upstream—a mechanism called rheotaxis (Miki & Clapham, 2013; El-Sherry *et al*, 2014; Kantsler *et al*, 2014; Tung *et al*, 2014, 2015; Bukatin *et al*, 2015). In the oviduct, long-range navigation via rheotaxis directs sperm to the site of fertilization (Miki & Clapham, 2013). An important ingredient of rheotaxis is the rotation of sperm around their longitudinal axis, called rolling (e.g., Miki & Clapham, 2013; Kantsler *et al*, 2014; Bukatin *et al*, 2015), resulting in a cone-shaped beating envelope. Through this mechanism, vertical shear flow, e.g., near boundary surfaces, exerts a torque that aligns the longitudinal axis of sperm against the flow direction (Miki & Clapham, 2013; Kantsler *et al*, 2014; Bukatin *et al*, 2015). However, whether sperm rolling involves full 360° or incomplete rotations of alternating direction is debated (Miki & Clapham, 2013; Muschol *et al*, 2018).

The intracellular Ca^{2+} concentration ($[Ca^{2+}]_i$) controls the flagellar beat and swimming behavior of sperm (Kaupp *et al*, 2003; Publicover *et al*, 2008; Fechner *et al*, 2015). In most sperm species, $[Ca^{2+}]_i$ is set by the voltage- and alkaline-activated CatSper Ca^{2+} channel (Quill *et al*, 2001; Ren *et al*, 2001; Kirichok *et al*, 2006; Lishko *et al*, 2010; Lishko *et al*, 2011; Strünker *et al*, 2011; Loux *et al*, 2013; Seifert *et al*, 2015). Mammalian CatSper comprises four homologous pore-forming subunits (CatSper 1–4) (e.g., Navarro *et al*, 2008) and at least six auxiliary subunits (CatSper β, γ, δ, ε, ζ, and Efcab9) (Liu *et al*, 2007; Wang *et al*, 2009; Chung *et al*, 2011, 2017; Hwang *et al*, 2019). The CatSper-channel complex is organized as quadrilateral threads along the flagellum; the CatSper threads encompass several other proteins, including

1 Centre of Reproductive Medicine and Andrology, University Hospital Münster, University of Münster, Münster, Germany
2 Optical Technologies Group, Institute of Applied Physics, University of Münster, Münster, Germany
3 Molecular Sensory Systems, Center of Advanced European Studies and Research, Bonn, Germany
4 Minerva Max Planck Research Group, Molecular Physiology, Center of Advanced European Studies and Research, Bonn, Germany
5 Institute of Innate Immunity, University Hospital, University of Bonn, Bonn, Germany
6 Institute of Human Genetics, University of Münster, Münster, Germany
7 Institute of Life Science and School of Life Science, Nanchang University, Nanchang, China
8 Cells-in-Motion Cluster of Excellence (EXC1003-CiM), Münster, Germany
*Corresponding author. Tel: +49 251 83 36160; E-mail: fallnich@uni-muenster.de
**Corresponding author. Tel: +49 251 83 58238; E-mail: timo.struenker@ukmuenster.de

Ca^{2+}-binding proteins and protein kinases, forming local Ca^{2+}-signaling domains near the membrane surface (Chung *et al*, 2014, 2017).

In *Catsper1*$^{-/-}$ mouse sperm, longitudinal rolling and rheotaxis were abolished (Miki & Clapham, 2013), suggesting that control of $[Ca^{2+}]_i$ by CatSper is required for rolling and rheotaxis of mammalian sperm. For human sperm, it was specifically proposed that rolling is created by asymmetrical Ca^{2+} influx via CatSper channels, stimulated by local pH_i signaling (Miller *et al*, 2018). The H^+ channel Hv1 is organized along the flagellum of human sperm in two threads near two of the four CatSper threads (Miller *et al*, 2018). It was proposed that H^+ efflux via Hv1 organizes localized Ca^{2+} signaling that, ultimately, creates an asymmetry in calcium-dependent inhibition of dynein-powered microtubule sliding (Miller *et al*, 2018). However, the concept that rolling and rheotaxis are enabled by Ca^{2+} influx cannot be reconciled with the finding that rolling of mouse sperm does not require extracellular Ca^{2+} (Babcock *et al*, 2014; Muschol *et al*, 2018), and that exposure of human sperm to gradients of flow velocities does not evoke measurable changes in $[Ca^{2+}]_i$ (Zhang *et al*, 2016). Moreover, the inventory and regulation of signaling molecules are different among mammalian sperm (Kaupp & Strünker, 2017). For example, mouse sperm lack Hv1 channels (Lishko *et al*, 2010; Berger *et al*, 2017), and human CatSper is activated by nanomolar concentrations of prostaglandins and progesterone (Lishko *et al*, 2011; Strünker *et al*, 2011) that do not activate mouse CatSper (Lishko *et al*, 2011). Thus, if the quadrilateral arrangement of CatSper and its control by pH_i were key to rolling and rheotaxis of mouse and human sperm, the underlying mechanisms ought to be vastly different.

Here, we show that human sperm undergo continuous full 360° rotations rather than incomplete rotations of alternating directions. Moreover, to scrutinize the role of CatSper and Ca^{2+} in rolling and rheotaxis of human sperm, we studied sperm of healthy donors and patients who suffer from the deafness-infertility syndrome (DIS). DIS patients lack the *CATSPER2* gene (Zhang *et al*, 2007; Hildebrand *et al*, 2010). We show by 3D-STORM that, in the absence of CatSper 2, other pore-forming CatSper subunits still assemble into quadrilateral threads of non-functional CatSper complexes. We demonstrate that rolling and rheotaxis persist in CatSper-deficient sperm from DIS patients. Furthermore, we show that rolling and rheotaxis of human sperm are preserved even when Ca^{2+} influx is completely abolished. Finally, we demonstrate that rolling and rheotaxis are also preserved in *Catsper1*$^{-/-}$ mouse sperm, which lack the CatSper complex and the quadrilateral threads altogether. We conclude that in mouse and human sperm, neither Ca^{2+} influx via CatSper nor the quadrilateral Ca^{2+}-signaling threads organized by CatSper are required for rolling and rheotaxis.

Results

The expression of pore-forming CatSper subunits is not strictly interdependent

We examined sperm from five infertile patients suffering from a homozygous deletion of contiguous genes on chromosome 15, including the *CATSPER2* gene (Fig EV1). This deletion at 15q15.3 is the hallmark of DIS (Zhang *et al*, 2007; Hildebrand *et al*, 2010). Motile sperm isolated from patients' ejaculates by the swim-up procedure were morphologically normal, but lacked CatSper-mediated Ca^{2+} influx (Fig 1A) and CatSper currents (Fig 1B and C), confirming that the deletion of the *CATSPER2* gene abrogates the expression of functional CatSper channels (Smith *et al*, 2013; Brenker *et al*, 2018a). Antibodies directed against CatSper 3 and CatSper 4 stained the principal piece of sperm from healthy donors and DIS patients (Fig 1D and E). 3D-STORM analysis revealed that the quadrilateral arrangement of CatSper 3 and CatSper 4 along the flagellum was preserved in DIS patients (Fig 1F and G). Thus, in the absence of CatSper 2, CatSper 3 and CatSper 4 subunits still assemble into non-functional protein complexes, whose sub-cellular arrangement is similar to that of the functional CatSper-channel complex (Chung *et al*, 2014, 2017).

Human sperm do not require functional CatSper channels for longitudinal rolling

We examined whether longitudinal rolling is impaired or even abolished in CatSper-deficient human sperm. Under dim dark-field illumination, we monitored rolling of sperm in population via periodic changes in brightness (blinking) of the sperm heads (Fig 2A–C; Movie EV1). Semi-automated analysis of blinking events revealed the rotation frequency of each sperm cell in the field of view. In non-capacitated and capacitated control sperm from healthy donors, the rotation frequency was normally distributed (Fig 2D) with a mean value of 4.8 ± 1.5 Hz (n = 1,455) and 7.0 ± 2.2 Hz (n = 1,097), respectively (Fig 2E) (Rigler & Thyberg, 1984; Aitken *et al*, 1985; Miller *et al*, 2018). Bicarbonate (25 mM) used for capacitation stimulates cAMP synthesis (Carlson *et al*, 2007; Tresguerres *et al*, 2011; Brenker *et al*, 2012) and, thereby, accelerates the flagellar beat (Esposito *et al*, 2004; Xie *et al*, 2006) and rotation frequency (Miki & Clapham, 2013). The rotation frequency decreased with increasing viscosity (Fig 2F), in line with previous results (e.g., Nosrati *et al*, 2015; Gallagher *et al*, 2019). To study rolling of single sperm cells with high time resolution and for long recording times, we combined bright-field microscopy with an optical tweezer (Ashkin *et al*, 1986) (Fig 2G). Sperm were trapped perpendicular to the optical axis (Fig 2H, Movie EV2), and the periodic intensity fluctuations of the laser light, which was back-scattered from the cell into the microscope objective, provided a measure of the rotation frequency (Fig 2I). For optically trapped control sperm from healthy donors, the rotation frequency was constant for several tens of seconds (Fig 2I). The frequency distribution and mean frequency of trapped sperm (6.0 ± 2.1 Hz, n = 32) and freely moving sperm (7.0 ± 2.2 Hz, n = 1,097) were similar (compare Fig 2J and D). Trapping of sperm parallel to the optical axis allowed a frontal view onto the tip of the sperm head; this view reveals that human sperm display continuous full 360° rotations (Fig 2K, Movie EV3), in contrast to incomplete rotations of alternating directions that have been reported for mouse sperm (Babcock *et al*, 2014; Muschol *et al*, 2018). Remarkably, also CatSper-deficient human sperm displayed longitudinal rolling (Movie EV4): In freely moving CatSper-deficient sperm incubated under non-capacitating or capacitating conditions, the rotation frequency was normally distributed around a mean value of 6.0 ± 2.6 Hz

(n = 1,009) and 6.8 ± 3.1 Hz (n = 946), respectively (Fig 2L and M). The CatSper-deficient human sperm swam progressively also in highly viscous media (Movie EV5), and, like in control sperm, the rotation frequency of CatSper-deficient sperm decreased with increasing viscosity (Fig 2N). When optically trapped, the CatSper-deficient sperm clearly displayed continuous full 360° rotations (Fig 2O and P, Movie EV6), and the rotation frequency remained constant over several tens of seconds (Fig 2Q). In conclusion, human sperm do not require functional CatSper for longitudinal rolling. If anything, the longitudinal rolling of CatSper-deficient sperm might be slightly enhanced in the absence of bicarbonate.

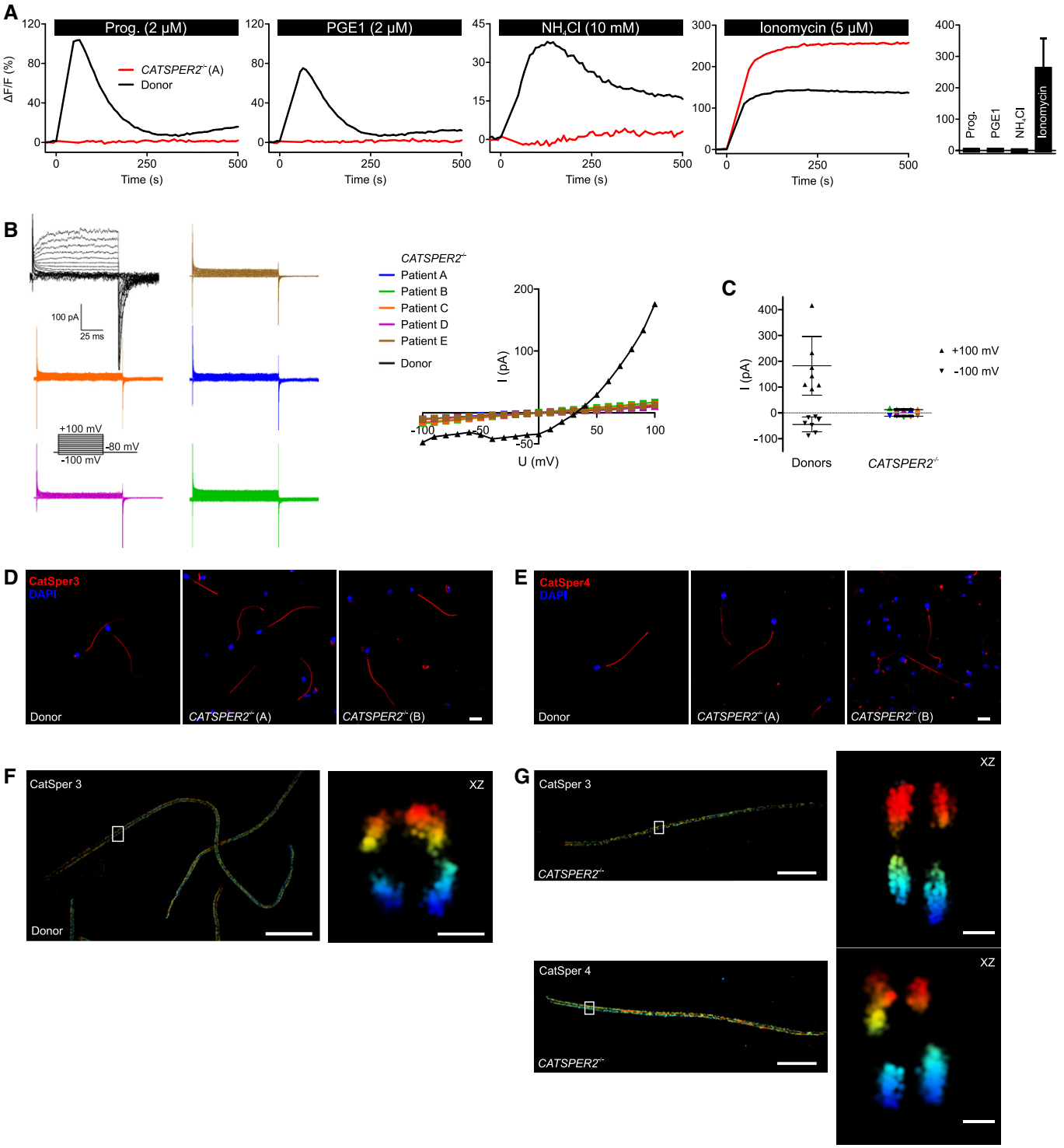

Figure 1.

Figure 1. Characterization of *CATSPER2*-deficient human sperm.

A Representative Ca^{2+} signals in sperm from a patient with deafness-infertility syndrome lacking functional CatSper channels (*CATSPER2*$^{-/-}$; red) and a healthy donor (black), evoked by progesterone, PGE1, NH_4Cl, or ionomycin. NH_4Cl increases the intracellular pH. Bar graph: Amplitudes (n = 4; mean ± SD) of Ca^{2+} signals in *CATSPER2*$^{-/-}$ sperm.

B Representative monovalent CatSper currents in *CATSPER2*$^{-/-}$ sperm (blue, green, orange, purple, brown) and in sperm from a healthy donor (black), and corresponding current-voltage relationship (right). The membrane voltage was stepped from −100 to +100 mV in increments of 10 mV from a holding potential of −80 mV.

C Outward and inward current amplitudes (mean ± SD) at + 100 mV and -100 mV, respectively, in *CATSPER2*$^{-/-}$ sperm (color code: panel B) and sperm from healthy donors (black).

D, E Representative immunocytochemical staining of control sperm from healthy donors and *CATSPER2*$^{-/-}$ sperm from DIS patients using antibodies directed against CatSper 3 (D) or CatSper 4 (E); DNA was labeled with DAPI (blue). Scale bars represent 10 μm.

F 3D-STORM image in xy projection of sperm from a healthy donor labeled with the anti-CatSper 3 antibody (left). Axial projection of the boxed region (right). Scale bars represent 5 μm in *xy* projections and 200 nm in axial projections.

G 3D-STORM images in xy projection of *CATSPER2*$^{-/-}$ sperm (left) labeled with the anti-CatSper 3 (upper panel) or anti-CatSper 4 (lower panel) antibody. Axial projection of the boxed regions (right). Scale bars represent 5 μm in *xy* projections and 200 nm in axial projections.

Longitudinal rolling of human sperm does not require an influx of Ca^{2+}

We further examined whether Ca^{2+} is required for rolling of human sperm, using both dark-field microscopy of sperm populations and optical trapping of single sperm cells. Control sperm from healthy donors held by the optical tweezer were dragged between parallel laminar flows of three different solutions (Figs 3A and EV2). This setup allows monitoring of the rotation frequency upon rapid switching of solutions. A stimulus buffer (stimulus stream) and sperm in control buffer (control stream) were separated by a barrier stream containing fluorescein in control buffer; the buffers were fed into a capillary via three inlets. The transfer from one to the other stream was monitored by changes in the fluorescence of fluorescein: When entering the barrier stream, the fluorescence rose and resumed basal values when sperm reached the stimulus stream (Fig 3B). Dragging of control sperm from healthy donors across the barrier stream was completed within ≤ 10 s (Movie EV7). Dragging itself did not affect rolling (Fig 3B and C): The mean rotation frequency before and after dragging between control buffers was 6.7 ± 2.8 Hz and 6.5 ± 2.8 Hz (n = 14), respectively. After dragging from bicarbonate-free to bicarbonate-containing buffer, the rotation frequency increased from 6.6 ± 2.9 to 11.3 ± 2.5 Hz (Fig 3D and E, n = 5). Next, the rotation frequency of trapped sperm cells before and after transition from 2 mM to < 20 nM extracellular Ca^{2+} was studied. The rotation frequency was similar in the absence and presence of Ca^{2+} (5.5 ± 3.6 Hz versus 5.9 ± 3.1 Hz, n = 5; Fig 3F and G). Although in dark-field microscopy of sperm populations, the fraction of motile sperm decreased in Ca^{2+}-free buffer with a time constant (τ) of 5.3 min (Fig 3H) (Aaberg *et al*, 1989; Jin *et al*, 2007; Torres-Flores *et al*, 2011), at any time-point during the decay, motile sperm were also rolling (Movie EV8). The

Figure 2. Analysis of longitudinal rolling of human sperm.

A Experimental setup for population analysis by dark-field microscopy.

B Dark-field microscopy of a single sperm cell; shown are single frames obtained at t = 0, 48, 96, and 136 ms. Scale bar = 25 μm.

C Dark-field imaging of a sperm population; left: single frames at t = 185, 363, 540, and 718 ms. Sperm selected for analysis are highlighted (1–4). Right: temporal change in the brightness (blinking) of sperm heads. The blue lines correspond to the time-points of the single frames. Scale bar = 25 μm.

D Representative distribution of rotation frequencies of freely swimming sperm incubated under non-capacitating (0 mM bicarbonate; black; n = 218) and capacitating (25 mM bicarbonate; red; n = 232) conditions determined by dark-field imaging.

E Rolling frequency (mean ± SD) of sperm incubated under non-capacitating (0 mM bicarbonate, n = 1,455; three experiments) and capacitating (25 mM bicarbonate, n = 1,097, eight experiments) conditions.

F Rolling frequency (mean ± SD) of freely swimming sperm in 0 (n = 1,175; five experiments), 0.2 (n = 832; three experiments), and 1% (n = 599; three experiments) methyl cellulose (w/v).

G Experimental setup for the laser-based optical tweezer.

H Bright-field images of an optically trapped sperm cell obtained at t = 0, 55, 155, and 185 ms. Scale bar represents 10 μm.

I Representative time-course of the rotation frequency of trapped sperm (each sperm cell is represented by a different color). Error bars indicate the full width at half prominence of the frequency peaks determined by the fast Fourier analysis.

J Distribution of rotation frequencies in trapped sperm (n = 32; mean frequency ± SD 6.0 ± 2.1 Hz).

K Image series of a sperm cell trapped parallel to the optical axis; images were obtained at t = 0, 95, 165, and 205 ms. The red bar indicates the 360° rotation of the tip of the head. Scale bar represents 10 μm.

L Representative distribution of rotation frequencies of freely swimming CatSper-deficient sperm incubated under non-capacitating (0 mM bicarbonate; black; n = 73) and capacitating conditions (25 mM bicarbonate; red; n = 272).

M Rolling frequency (mean ± SD) of freely swimming *CATSPER2*$^{-/-}$ sperm incubated under non-capacitating (0 mM bicarbonate, n = 1,009; four experiments) and capacitating (25 mM bicarbonate, n = 946; seven experiments) conditions.

N Rolling frequency (mean ± SD) of freely swimming *CATSPER2*$^{-/-}$ sperm in 0 (n = 457; four experiments), 0.2 (n = 389; two experiments), and 1% (n = 187; two experiments) methyl cellulose (w/v).

O Image series of a *CATSPER2*$^{-/-}$ sperm cell optically trapped perpendicular to the optical axis; images were obtained at t = 0, 75, 150, and 225 ms. Scale bar represents 10 μm.

P Image series of a *CATSPER2*$^{-/-}$ sperm cell optically trapped parallel to the optical axis; images were obtained at t = 0, 60, 195, and 320 ms. The red bar indicates the 360° rotation of the tip of the head. Scale bar represents 10 μm.

Q Representative time courses of the rotation frequencies of optically trapped *CATSPER2*$^{-/-}$ sperm (each sperm is represented in a different color). Error bars indicate the full width at half prominence of the frequency peaks determined by the fast Fourier analysis.

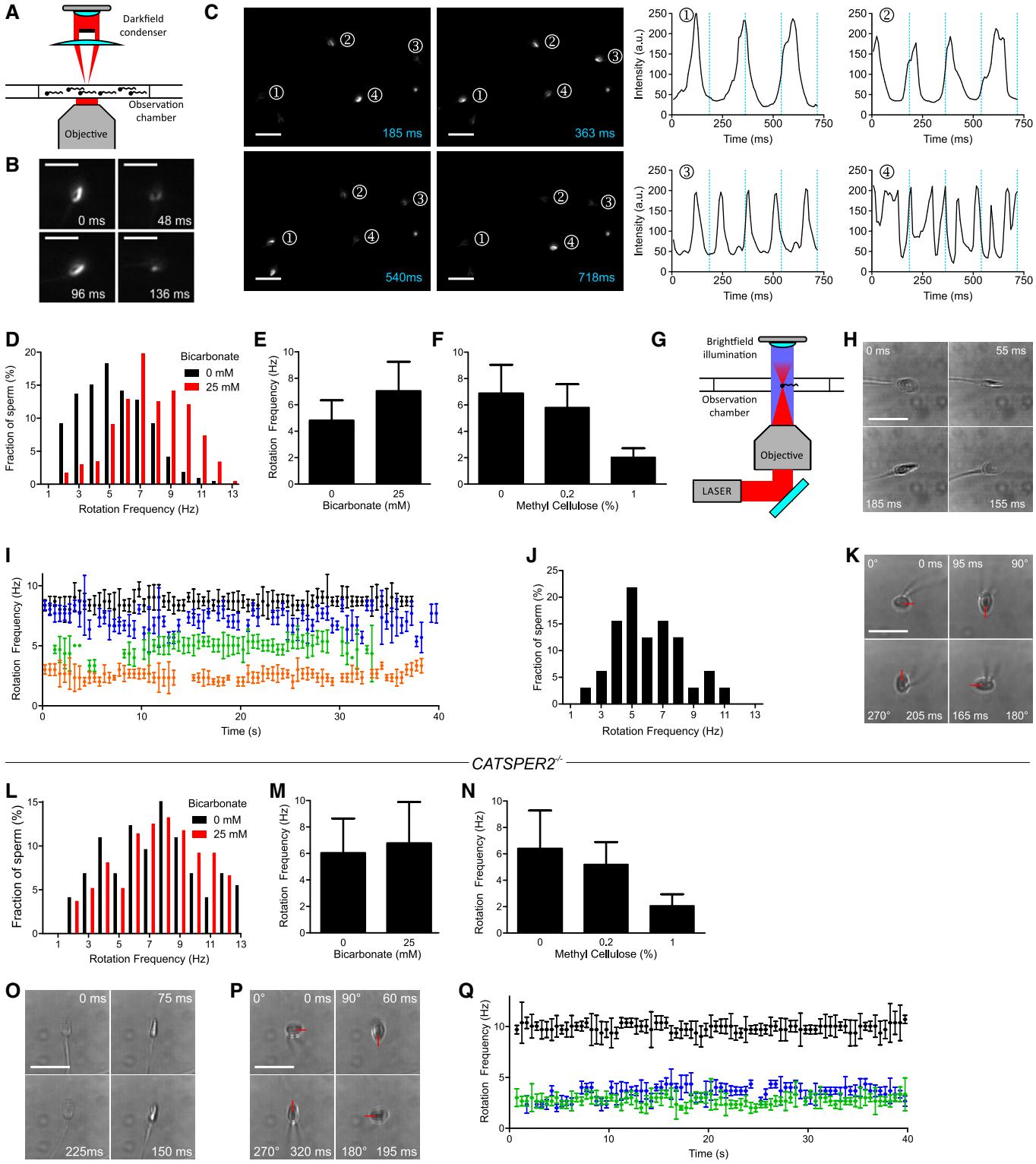

Figure 2.

mean rotation frequency and the rotation frequency-histogram (determined at ≤ 5 min in Ca^{2+}-free buffer) were similar to those under control conditions (6.3 ± 1.9 Hz, n = 224; Fig 3I). These results show that Ca^{2+} influx is not required for rolling of human sperm.

CatSper-deficient human sperm display rheotaxis

Next, we studied the swimming behavior of human sperm in a glass capillary with and without fluid flow. Sperm were tracked in the field of view, and the starting point of each track was shifted to the origin

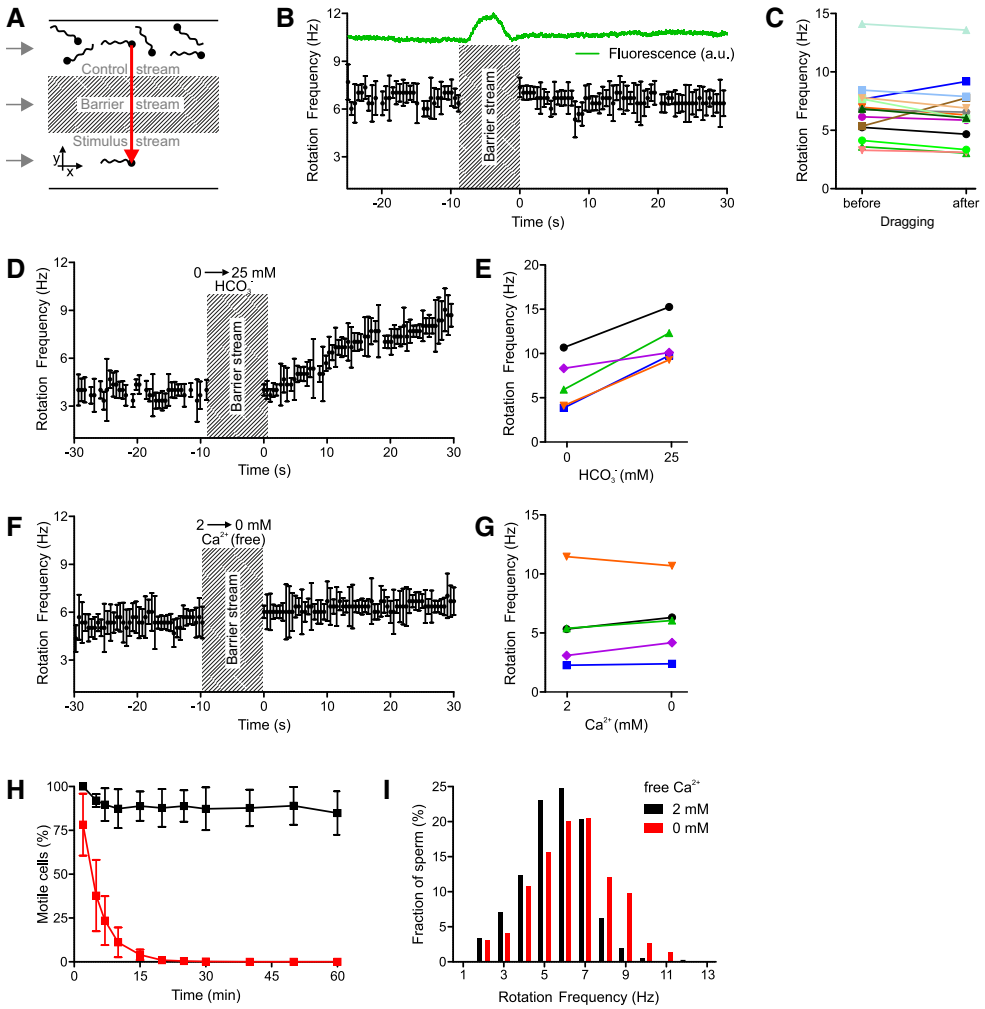

Figure 3. The action of bicarbonate and Ca^{2+} on longitudinal rolling of human sperm.

A Experimental setup to subject optically trapped sperm to different conditions in a three-channel microfluidic capillary.

B Rotation frequency of a trapped sperm cell before and after dragging across the barrier stream. The green trace indicates the fluorescence of fluorescein included in the barrier stream. Error bars indicate the full width at half prominence of the frequency peaks determined by the fast Fourier analysis.

C Paired plot of rotation frequencies of individual sperm cells before and after dragging across the barrier stream.

D Rotation frequency of a trapped sperm cell before and after dragging from the control stream containing 0 mM bicarbonate into the stimulus stream containing 25 mM bicarbonate. Error bars indicate the full width at half prominence of the frequency peaks determined by the fast Fourier analysis.

E Paired plot of rotation frequencies of individual sperm at 0 and 25 mM bicarbonate.

F Rotation frequency of a trapped sperm cell in the presence and absence of extracellular Ca^{2+}. Error bars indicate the full width at half prominence of the frequency peaks determined by the fast Fourier analysis.

G Paired plot of rotation frequencies in the presence and absence of extracellular Ca^{2+}.

H Fraction of motile sperm (mean ± SD) in a sperm population incubated in the presence (black) and absence (at t = 0) of extracellular Ca^{2+} (red; $n \geq 5$).

I Distribution of rotation frequencies in populations of freely swimming sperm in the presence (black, n = 335) and absence (red, n = 224) of extracellular Ca^{2+}.

of a coordinate system (Fig 4A, C, E, G, I, K). To quantify the rheotactic behavior, we determined the angular swimming directions and plotted the mean relative frequency of sperm swimming with angular directions of 45°–135°, 135°–225°, 225°–315°, and 315°–45° in a spider plot. Under no-flow conditions, control sperm swam randomly without any preferred directional angle (Fig 4A and B). In contrast, under flow conditions, a large fraction of sperm aligned their swimming path against the flow direction (Fig 4C and D, angular direction of the flow = 0°). The fraction of sperm swimming with directional angles between 135° and 225° was 25.7 ± 1.7% (n = 7, 1,301 sperm) and 44.3 ± 8.6% (n = 7, 1,083 sperm) in the absence and presence of a flow, respectively. For CatSper-deficient sperm under no-flow conditions, the angular swimming directions were random (Fig 4E and F; Movie EV9). Under flow conditions, like in control sperm, a large fraction of the CatSper-deficient sperm aligned their swimming path against the flow direction (Fig 4G and H; Movie EV10). The fraction of CatSper-deficient sperm swimming with directional angles between 135° and 225° was 27.6 ± 1.8% (no-flow; n = 6, 1,068 sperm) versus 47.8 ± 3.4% (flow; n = 7, 1,068 sperm). These results demonstrate that functional CatSper channels are dispensable not only for rolling, but also for rheotaxis of human sperm.

Rheotaxis of human sperm does not require Ca^{2+} influx

Finally, we studied the trajectories of CatSper-deficient sperm in Ca^{2+}-free buffer ($[Ca^{2+}] < 20$ nM). Under no-flow conditions, the angular swimming directions were random (Fig 4I and J). Under flow conditions, like in the presence of extracellular Ca^{2+}, a large fraction of the CatSper-deficient sperm aligned their swimming path against the flow direction (Fig 4K and L); in Ca^{2+}-free buffer, the fraction of CatSper-deficient sperm swimming with directional angles between 135° and 225° was 28.2 ± 2.7% (no-flow; $n = 4$, 442 sperm) versus 43.3 ± 3.6% (flow; $n = 4$, 620 sperm). These results demonstrate that Ca^{2+} influx in general is dispensable for both rolling and rheotaxis of human sperm and that rheotaxis of CatSper-deficient human sperm is similar in the absence and presence of extracellular Ca^{2+}.

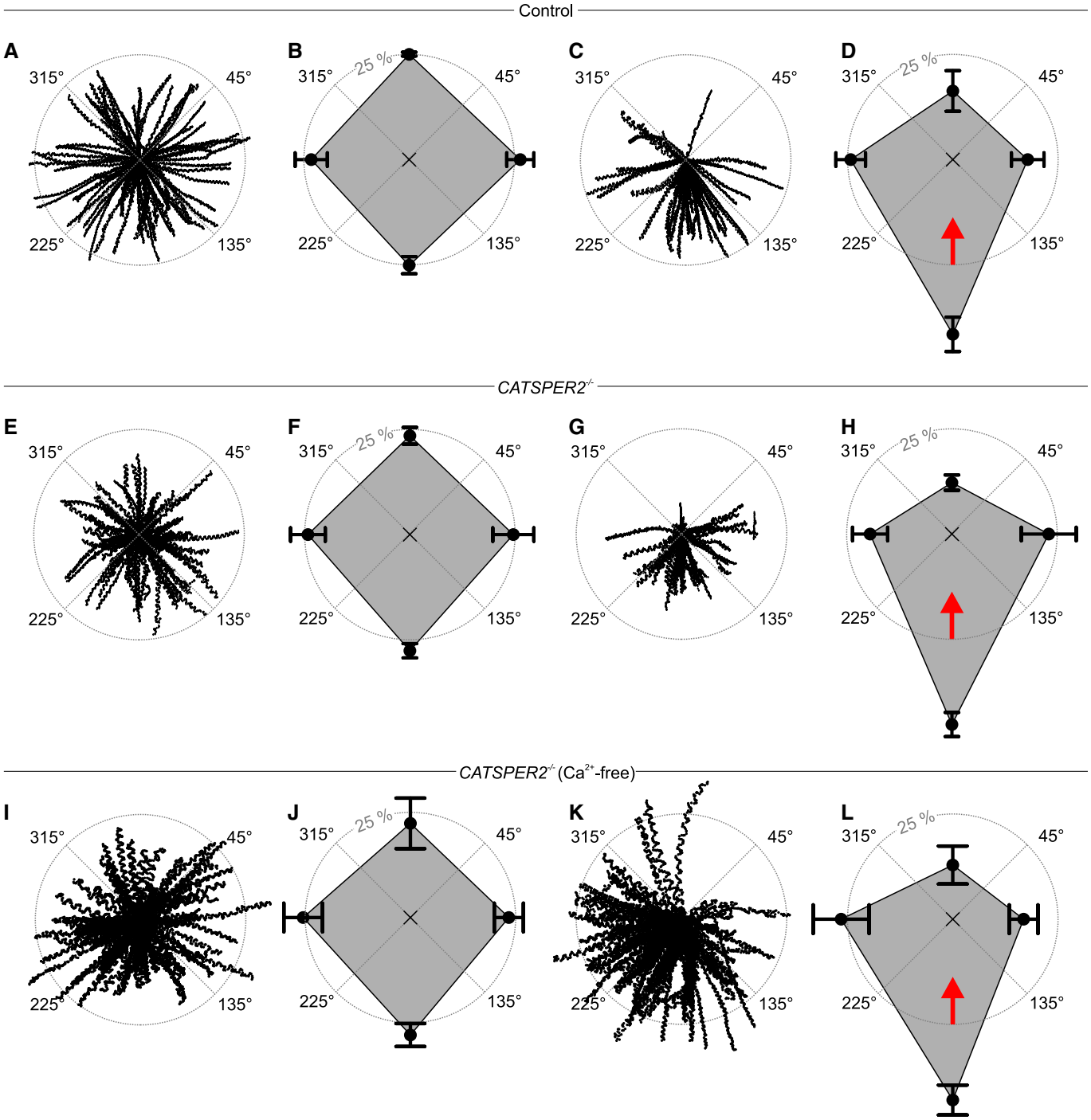

Figure 4.

Figure 4. Rheotaxis of human sperm.

A Trajectories of human sperm in the absence of a fluid flow. Sperm were tracked for 1.86 s. The starting point of each trajectory was centered to the origin of a coordinate system, represented by the intersection of the dotted lines in the center of the circle.

B Spider-web plot of the mean (± SD) relative frequencies of sperm swimming with an angular direction of 315°–45°, 45°–135°, 135°–225°, and 225°–315° (n = 7; 1,301 sperm) in the absence of a fluid flow.

C Representative trajectories of human sperm in the presence of a fluid flow.

D Spider-web plot of the mean (± SD) relative frequencies of angular swimming directions (n = 7; 1,083 sperm) in the presence of a fluid flow. The red arrow indicates the flow direction.

E Representative trajectories of *CATSPER2*$^{-/-}$ sperm in the absence of a fluid flow.

F Spider-web plot of the mean (± SD) relative frequencies of angular swimming directions of *CATSPER2*$^{-/-}$ sperm in the absence of a fluid flow (n = 6; 1,068 sperm).

G Trajectories of *CATSPER2*$^{-/-}$ sperm in the presence of a fluid flow.

H Spider-web plot of the mean (± SD) relative frequencies of angular swimming directions of *CATSPER2*$^{-/-}$ sperm in the presence of a fluid flow (n = 7; 1,068 sperm). The red arrow indicates the fluid flow direction.

I Representative trajectories of *CATSPER2*$^{-/-}$ sperm in Ca^{2+}-free buffer in the absence of a fluid flow.

J Spider-web plot of the mean (± SD) relative frequencies of angular swimming directions (n = 4; 442 sperm) of *CATSPER2*$^{-/-}$ sperm in Ca^{2+}-free buffer in the absence of a fluid flow.

K Representative trajectories of *CATSPER2*$^{-/-}$ sperm in Ca^{2+}-free buffer in the presence of a fluid flow.

L Spider-web plot of the mean (± SD) relative frequencies of angular swimming directions (n = 4; 620 sperm) of *CATSPER2*$^{-/-}$ sperm in Ca^{2+}-free buffer in the presence of a fluid flow. The red arrow indicates the flow direction.

Rolling and rheotaxis persist in CatSper-deficient mouse sperm

Although both devoid of functional CatSper channels, rolling and rheotaxis are largely unaffected in human *CATSPER2*$^{-/-}$ sperm, but seem to be abolished in mouse *Catsper1*$^{-/-}$ sperm (Miki & Clapham, 2013). A major difference is that the quadrilateral Ca^{2+}-signaling threads are disrupted in *Catsper1*$^{-/-}$ mouse sperm (Chung *et al*, 2014), but not in *CATSPER2*$^{-/-}$ human sperm (Fig 1G). This finding suggests that the supramolecular CatSper organization might be required for rolling and rheotaxis. To test for this possibility, we re-examined rolling and rheotaxis in mouse *Catsper1*$^{-/-}$ sperm. Surprisingly, not only wild-type (Fig 5A, Movie EV11) but also *Catsper1*$^{-/-}$ sperm (Fig 5B, Movie EV12) clearly displayed longitudinal rolling. The mean rotational frequency of wild-type and *Catsper1*$^{-/-}$ sperm was 2.9 ± 1.3 Hz (n = 24) and 2.6 ± 0.7 Hz (n = 24), respectively (Fig 5A and B). We studied the swimming behavior of wild-type and *Catsper1*$^{-/-}$ mouse sperm in a glass capillary with and without fluid flow. We tracked sperm in the field of view, and the starting point of each track was shifted to the origin of a coordinate system (Fig 5C, E, G, I). To quantify the rheotactic behavior, we determined the angular swimming directions and plotted the mean relative frequencies of sperm swimming with an angular direction of 45°–135°, 135°–225°, 225°–315°, and 315°–45° in a spider plot. Under no-flow conditions, wild-type mouse sperm swam randomly without any preferred directional angle (Fig 5C and D). In contrast, under flow conditions, a large fraction of sperm aligned their swimming path against the flow direction (Fig 5E and F; angular direction of the flow = 0°). The fraction of sperm swimming with directional angles between 135° and 225° was 25.6 ± 5.9% (n = 3, 127 sperm) and 53.2 ± 6.7% (n = 3, 175 sperm) in the absence and presence of flow, respectively (see also Movies EV13 and EV14). For *Catsper1*$^{-/-}$ mouse sperm under no-flow conditions, the angular swimming directions were random (Fig 5G and H, Movie EV15). Under flow conditions, like in wild-type sperm, a large fraction of *Catsper1*$^{-/-}$ sperm aligned their swimming path against the flow direction (Fig 5I and J, Movie EV16). The fraction of *Catsper1*$^{-/-}$ sperm swimming with directional angles between 135° and 225° was 26.0 ± 1.5% (no-flow; n = 4, 297 sperm) versus 44.2 ± 10.9% (flow; n = 4, 261 sperm), respectively. These results demonstrate that also rolling and rheotaxis of mouse sperm

Figure 5. Rolling behavior and rheotaxis of mouse sperm.

A Left: Bright-field image series of a freely swimming wild-type sperm cell at t = 0, 151, and 303 ms. Scale bar represents 10 μm. Right: rotation frequency (mean ± SD) of freely swimming wild-type sperm (n = 24, three experiments).

B Left: Bright-field image series of a freely swimming *Catsper1*$^{-/-}$ sperm cell at t = 0, 151, and 294 ms. Scale bar represents 10 μm. Right: rotation frequency (mean ± SD) of freely swimming *Catsper1*$^{-/-}$ sperm (n = 24, three experiments).

C Representative trajectories of wild-type sperm in the absence of a fluid flow. The starting point of each trajectory was centered to the origin of a coordinate system, represented by the intersection of the dotted lines in the center of the circle. Each color represents one trajectory.

D Spider-web plot of the mean (± SD) relative frequencies of sperm swimming with an angular direction of (binning: 315°–45°, 45°–135°, 135°–225°, and 225°–315° (n = 3; 127 sperm) in the absence of a fluid flow.

E Representative trajectories of wild-type sperm in the presence of a fluid flow.

F Spider-web plot of the mean (± SD) relative frequencies of angular swimming directions (n = 3; 175 sperm) of wild-type sperm in the presence of a fluid flow. The red arrow indicates the flow direction.

G Representative trajectories of *Catsper1*$^{-/-}$ sperm in the absence of a fluid flow. The starting point of each trajectory was centered to the origin of a coordinate system, represented by the intersection of the dotted lines in the center of the circle. Trajectories are magnified by a factor of 2.05 with respect to the plots C and E to compensate for the reduced swimming speed of the *Catsper1*$^{-/-}$ sperm.

H Spider-web plot of the mean (± SD) relative frequencies of angular swimming directions of *Catsper1*$^{-/-}$ sperm (n = 4; 297 sperm) in the absence of a fluid flow.

I Representative trajectories of *Catsper1*$^{-/-}$ sperm in the presence of a fluid flow; trajectories are magnified by a factor of 2.05 with respect to the plots C and E to compensate for the reduced swimming speed of the *Catsper1*$^{-/-}$ sperm, and two trajectories were truncated (indicated by two parallel lines).

J Spider-web plot of the mean (± SD) relative frequencies of angular swimming directions (n = 4; 261 sperm) of *Catsper1*$^{-/-}$ sperm in the presence of a fluid flow. The red arrow indicates the flow direction.

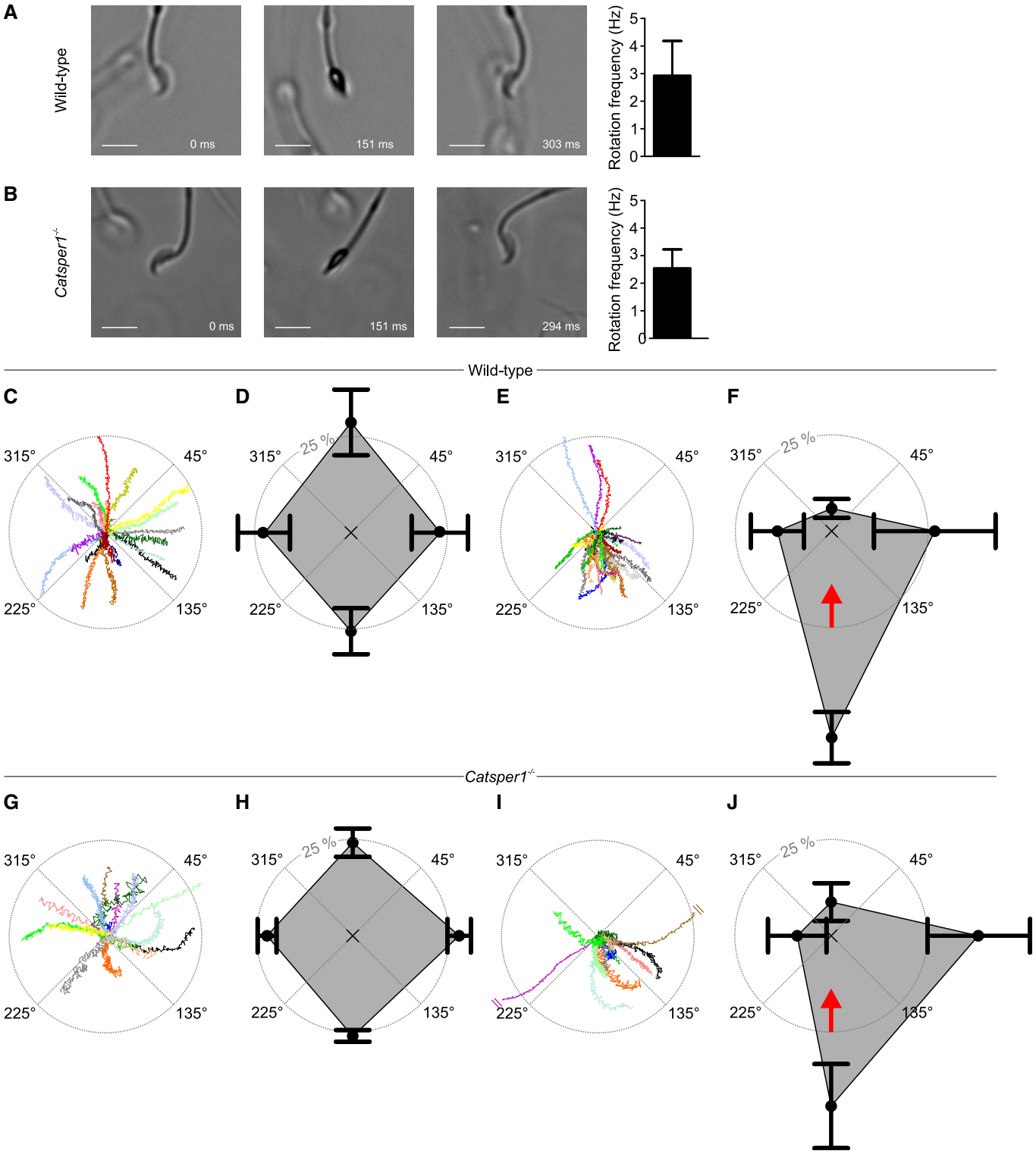

Figure 5.

do not require functional CatSper channels. For the time being, we cannot reconcile ours with previous results (Miki & Clapham, 2013). We suggest that other laboratories examine rolling and rheotaxis of CatSper-deficient mouse sperm independently.

Discussion

The Ca^{2+} channel CatSper has been implicated in rolling and rheotactic steering of mammalian sperm (Miki & Clapham, 2013;

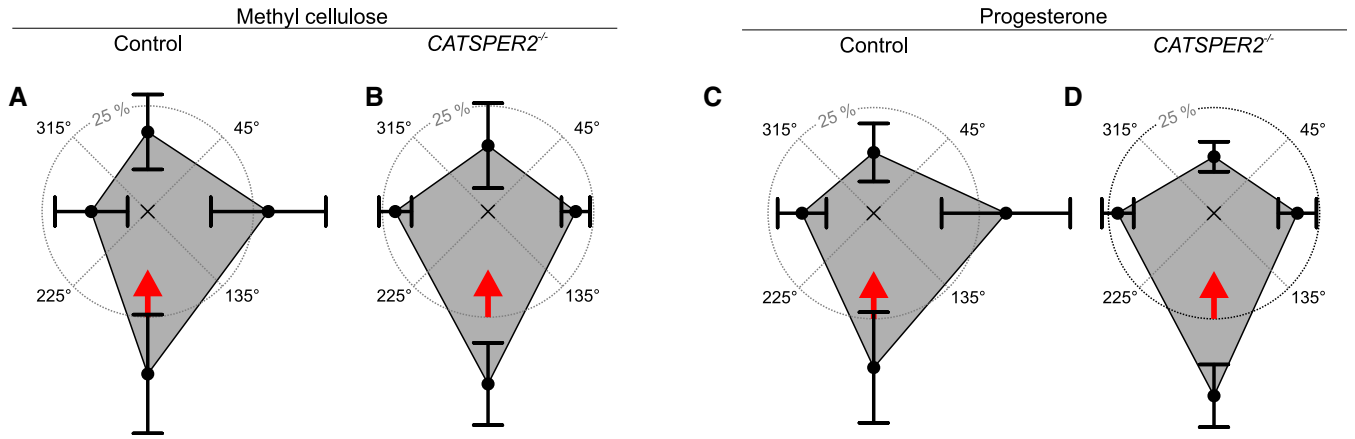

Figure 6. Rheotaxis of human sperm in viscous media and in the presence of progesterone.

A Spider-web plot of the mean (± SD) relative frequencies of sperm swimming with an angular direction of 315°–45°, 45°–135°, 135°–225°, and 225°–315° (n = 3; 403 sperm) of human sperm swimming in buffer fortified with 0.2% (w/v) methyl cellulose in the presence of a fluid flow.

B Spider-web plot of the mean (± SD) relative frequencies of angular swimming directions (n = 3; 520 sperm) of human *CATSPER2*$^{-/-}$ sperm swimming in buffer fortified with 0.2% (w/v) methyl cellulose in the presence of a fluid flow.

C Spider-web plot of the mean (± SD) relative frequencies of sperm swimming with an angular direction of 315°–45°, 45°–135°, 135°–225°, and 225°–315° (n = 3; 454 sperm) of human sperm swimming in buffer fortified with 100 nM progesterone in the presence of a fluid flow.

D Spider-web plot of the mean (± SD) relative frequencies of angular swimming directions (n = 3; 372 sperm) of human *CATSPER2*$^{-/-}$ sperm swimming in buffer fortified with 100 nM progesterone in the presence of a fluid flow. Data information: The red arrow indicates the flow direction.

Miller *et al*, 2018). We show that, in fact, rolling and rheotaxis of both human and mouse sperm do not require Ca^{2+} influx via CatSper. This conclusion agrees with other reports: Rolling of mouse sperm does not require extracellular Ca^{2+} (Babcock *et al*, 2014; Muschol *et al*, 2018), and exposure of human sperm to gradients of flow velocities does not evoke measurable changes in $[Ca^{2+}]_i$ (Zhang *et al*, 2016). Furthermore, it has been proposed that the quadrilateral organization of CatSper and associated signaling components provides the flagellar ultrastructure required for rolling and rheotaxis (Miller *et al*, 2018). The CatSper complex and the quadrilateral Ca^{2+}-signaling domains are abolished in *Catsper1*$^{-/-}$ mouse sperm (Chung *et al*, 2014), but not in human *CATSPER2*$^{-/-}$ sperm. Yet, both sperm species display rheotaxis and undergo rolling, suggesting that also the quadrilateral flagellar architecture along with potential asymmetric cytosolic Ca^{2+} gradients established by this structure is dispensable. Furthermore, mouse sperm lack Hv1 channels (Lishko *et al*, 2010; Berger *et al*, 2017), indicating that asymmetrical, spatially confined pH gradients established by Hv1 are not required for rolling and rheotaxis. Altogether, our results strongly support the concept that passive biomechanical and hydrodynamic processes enable rolling and rheotaxis rather than active spatio-temporally confined Ca^{2+} and H^+ signaling.

On a broader perspective, rolling is not a unique feature of sperm that undergo rheotaxis: Sperm from marine external fertilizers also exhibit longitudinal rolling (Jikeli *et al*, 2015), although in their aquatic habitat, no gradients of fluid velocity exist and chemotaxis rather than rheotaxis is employed for navigation.

Of note, even in a viscous medium, rheotaxis of CatSper-deficient and healthy human sperm was rather similar (Fig 6A and B). Thus, at the particular flow velocity and viscosity that we used, and with respect to the parameters that we analyzed, the lack of functional CatSper does not seem to affect rheotaxis in more viscous fluid. However, human sperm display rheotaxis within a broad range of physiological flow velocities and viscosities (Kantsler *et al*, 2014). The relation of upstream versus shear velocity is bell-shaped (Kantsler *et al*, 2014), demonstrating that the rheotactic performance peaks at a particular shear profile. Furthermore, the trajectories of human sperm swimming against a flow feature a transverse component, and in cylindrical tubes, sperm swim on spiral-shaped trajectories along the walls, thereby exploring the tube's surface (Kantsler *et al*, 2014). The transversal component is positively and negatively related to the shear velocity and viscosity, respectively. Thus, subtle differences in the 3D beat of CatSper-deficient sperm might compromise rheotactic performance under some conditions encountered in the oviduct. For example, rheotaxis might be compromised at certain shear velocities and/or fluid viscosities, the relationship of upstream versus shear velocity might be shifted, and/or the transversal component might be altered. The beat envelope is a critical determinant of the rheotactic performance: Mouse sperm that lack CatSper ζ suffer from a rather stiff proximal flagellum, altering the 3D flagellar envelope and hamper the reorientation in fluid flow (Chung *et al*, 2017). Future studies need to quantify the 3D flagellar beating pattern of control versus CatSper-deficient human sperm as well as their rheotactic performance over a broad range of fluid flows and viscosities.

Furthermore, in human sperm, CatSper translates stimulation with oviductal hormones, like steroids and prostaglandins (Lishko *et al*, 2011; Strünker *et al*, 2011; Brenker *et al*, 2012, 2018a; Miller *et al*, 2016; Mannowetz *et al*, 2017), into Ca^{2+} and motility responses that are important for human sperm chemotaxis and hyperactivation (Schaefer *et al*, 1998; Harper *et al*, 2003; Oren-Benaroya *et al*, 2008; Publicover *et al*, 2008; Baldi *et al*, 2009; Kilic *et al*, 2009; Alasmari *et al*, 2013; Schiffer *et al*, 2014; Tamburrino *et al*, 2014, 2015; Rennhack *et al*, 2018). In the absence and

presence of progesterone (100 nM), rheotaxis of control and CatSper-deficient human sperm was rather similar (Fig 6C and D), indicating that under our conditions, progesterone activation of CatSper does not affect rheotaxis. However, to decipher how the ligand control of CatSper and, thereby, $[Ca^{2+}]_i$ are intertwined with rheotaxis, it is required to quantify rheotaxis of control and CatSper-deficient human sperm in the absence and presence of pico- to micromolar progesterone concentrations over a broad range of flow velocities and viscosities that emulate *in vitro* the complex physicochemical landscape of the oviduct.

On a final note, it is unknown whether sub- or infertility in men correlates with the failure of sperm to undergo rheotaxis. Studying rheotaxis is technically demanding. Therefore, we propose to assess longitudinal rolling as a surrogate biomarker for infertility. The population analysis introduced in this study can be readily incorporated into existing computer-assisted sperm analysis setups for clinical diagnostics.

Materials and Methods

Reagents

Reagents were obtained from Sigma-Aldrich (USA) unless otherwise indicated.

Sperm preparation and buffer conditions

The studies were performed in accordance with the standards set by the Declaration of Helsinki. Samples of human semen were obtained from healthy volunteers and DIS patients with their prior written consent, under approval of the institutional ethical committees of the medical association Westfalen-Lippe and the medical faculty of the University of Münster (4INie). Ejaculates were allowed to liquefy at 37°C for 30–60 min. Motile sperm were purified by a "swim-up" procedure: Liquefied semen (0.5–1 ml) was layered in a 50-ml Falcon tube below 4 ml of human tubal fluid (HTF) medium containing (in mM): 93.8 NaCl, 4.69 KCl, 0.2 $MgSO_4$, 0.37 KH_2PO_4, 2.04 $CaCl_2$, 0.33 Na-pyruvate, 21.4 lactic acid, 2.78 glucose, 4 $NaHCO_3$, and 21 HEPES, pH 7.35 (adjusted with NaOH). Alternatively, the semen was diluted 1:10 with HTF and sperm, somatic cells, and cell debris were pelleted by centrifugation at 700 *g* for 20 min (37°C). The pellet was resuspended in the same volume HTF, 50-ml Falcon tubes were filled with 5 ml of the suspension, and cells were pelleted by centrifugation at 700 *g* for 5 min (37°C). In either case, motile sperm were allowed to swim up into HTF for 60–90 min at 37°C. After swim-up, sperm were washed twice (700 *g*, 20 min) with HTF, the sperm concentration was adjusted, and HTF was supplemented with 3 mg/ml human serum albumin (HSA, Scientific Irvine, USA; referred to as HTF^+); under these conditions, sperm are non-capacitated. For capacitation, sperm were resuspended after the second wash in HTF^{++} medium, containing (in mM): 72.8 NaCl, 4.69 KCl, 0.2 $MgSO_4$, 0.37 KH_2PO_4, 2.04 $CaCl_2$, 0.33 Na-pyruvate, 21.4 lactic acid, 2.78 glucose, 25 $NaHCO_3$, and 21 HEPES, pH 7.35 (adjusted with NaOH), and supplemented with 3 mg/ml HSA. Sperm were capacitated in HTF^{++} for at least 3 h. Alternatively, swim-up and washing were directly performed in HTF^{++}. To study non-capacitated sperm in the absence of bicarbonate and the motility response evoked by a step increase in bicarbonate, swim-up and washing were performed in bicarbonate-free HTF containing (in mM): 97.8 NaCl, 4.69 KCl, 0.2 $MgSO_4$, 0.37 KH_2PO_4, 2.04 $CaCl_2$, 0.33 Na-pyruvate, 21.4 lactic acid, 2.78 glucose, and 21 HEPES, pH 7.35 (adjusted with NaOH). HSA (3 mg/ml) was added prior to the experiment to prevent attaching of sperm to the surface of the recording chamber. C57BL/6 wild-type and *Catsper1*$^{-/-}$ mice were handled and sacrificed in accordance with the German Animal Welfare Act and the district veterinary office under approval by the LANUV (84-02.05.20.13.115). Mouse epididymis was obtained from at least 21-week-old male mice that were anaesthetized with CO_2 or isoflurane (AbbVie Deutschland, Ludwigshafen, Germany) and sacrificed by cervical dislocation. Mouse sperm were isolated by incision of the cauda epididymis in modified TYH medium containing (in mM): 138 NaCl, 4.8 KCl, 2 $CaCl_2$, 1.2 KH_2PO_4, 1 $MgSO_4$, 5.6 glucose, 0.5 sodium pyruvate, 10 sodium DL-lactate, and 10 HEPES, pH 7.4. Sperm were allowed to swim out for 30 min at 30°C and 10% CO_2. *Catsper1*$^{-/-}$ mice (Ren *et al*, 2001) were generously provided by David Clapham (Janelia Research Campus, USA).

Rolling analysis in sperm populations

The longitudinal rolling of human sperm was recorded in glass chambers (depth of ~ 100 μm) under an inverted microscope (IX73; Olympus, Germany), equipped with a condenser (IX2-LWUCD; Olympus, Germany) with a custom-made dark-field filter, a 10× objective (UPLFLN10X2PH1; Olympus, Germany), and additional 1.6× magnification lenses (16× final magnification). The samples were illuminated with a red light-emitting diode (LED; M660D2; Thorlabs, Germany) and a custom-made power supply. To study sperm rolling in bicarbonate-free HTF or HTF^{++}, sperm were diluted 1:9 in the respective buffer 5–30 min prior to the experiment. To study rolling in the absence of extracellular Ca^{2+} ($[Ca^{2+}]_o < 20$ nM), sperm in HTF^{++} were diluted 1:9 only prior to the experiment into a Ca^{2+}-free HTF medium (HTF^{0Ca}), containing (in mM): 69.8 NaCl, 4.69 KCl, 0.2 $MgSO_4$, 0.37 KH_2PO_4, 5 EGTA, 0.33 Na-pyruvate, 21.4 lactic acid, 2.78 glucose, 25 $NaHCO_3$, and 21 HEPES, pH 7.35 (adjusted with NaOH), and supplemented with 3 mg/ml HSA. To study sperm rolling in viscous medium, sperm in HTF^+ were diluted in HTF^+ fortified with methyl cellulose. Over 4–10 min, short movies (~ 725 ms) of sperm in different fields of view in the observation chamber were recorded at 124 Hz with a high-speed sCMOS camera (Zyla, 4.2 plus, Andor, UK). Longitudinal rolling was assessed with a custom-made program written in the ImageJ macro language (Rasband, 1997–2016). In brief, moving sperm heads were tracked, and rotation was monitored by an oscillating change in head brightness. The rotation frequency was computed from the average temporal distance between two intensity peaks. The sperm head is approximately plane symmetrical with planes intersecting the length axis and, therefore, lights up twice per 360° rotation. Thus, the rotation frequency (F_{Rot}) is given by $F_{Rot} = F_{Blink} \times 0.5$. Sperm that displayed less than three relative maxima within the observation time were excluded from the analysis, yielding a cut-off for F_{Rot} of about 1.5 Hz; immotile sperm were excluded from the analysis. The rolling of mouse sperm in TYH was studied in observation chambers (depth of ~ 400 μm; Ibidi, Germany) under an

inverted microscope (IX73; Olympus, Germany) equipped with a condenser (IX2-LWUCD; Olympus, Germany), a 10× objective (UPLFLN10X2PH1, Olympus, Germany), and, optionally, an additional 1.6× magnification lens. The sample was illuminated by a red LED (M660D2; Thorlabs, Germany). Movies of sperm were recorded with a high-speed sCMOS camera (Zyla, 4.2 plus; Andor, UK). The rolling frequency of sperm was determined by visual frame-by-frame analysis.

Optical trapping of sperm

Unless otherwise indicated, we used capacitated sperm in HTF^{++} for optical-trapping experiments. The trapping of sperm cells was achieved with an optical tweezer (Ashkin *et al*, 1986; Fig EV2), using a continuous-wave (cw) diode laser (Lumics LU0975M500, Germany) at a wavelength of 976 nm (red beam in Fig EV2). The laser beam was expanded by a telescope setup of two lenses (L) to a diameter of 1.7 mm (full width at half maximum) and directed into a 100× oil immersion objective (MO, Plan-Apochromatic 100×/1.40 Oil DIC M27, Zeiss, Germany) with a numerical aperture (NA) of 1.4, allowing for tight focusing of the laser beam onto the head of a sperm swimming inside an observation capillary. To assess the rotation frequency of trapped sperm, the laser light reflected by the sperm head into the objective was directed onto a photomultiplier tube (PMT, H10721-20, Hamamatsu, Japan) by a beam splitter (reflectivity ~ 4%). A long-pass filter in front of the PMT blocked both the bright-field illumination and ambient light. The PMT signal was sampled with a frequency of 2 kHz, and every 10 points were averaged. The rotation frequency was determined by a fast Fourier transformation in a moving time window of 1.5 s. In parallel to the quantification of the back-reflected laser light, we recorded the trapped sperm with a bright-field microscope. A blue LED, equipped with a 450-nm short-pass filter (SP) and a collimator lens, served as a light source (blue beam in Fig EV2). The bright-field image was reflected by a dichroic mirror (DM), projected by a lens onto the chip of a charge-coupled device (CCD) camera (UI-3140CP-M-GL, IDS, Germany) and recorded with a frame rate of 200 Hz. To measure the rotation frequency of a sperm at different conditions, we trapped sperm inside a microfluidic capillary (dimensions [height × width]: 0.4 × 0.33 μm; μ-Slide III 3in1; Ibidi, Germany) with three separate inlets to establish a continuous, parallel laminar flow of three solutions ((i) control stream with sperm, (ii) barrier stream, and (iii) stimulus stream) with a flow speed of 65 μm/s. The barrier stream was supplemented with fluorescein (1 μM). Fluorescein was excited with the blue LED; fluorescence light was collected through the microscope objective and reflected by two DMs through a long-pass filter onto a second PMT (H10721-210; Hamamatsu, Japan). Using a custom-built mechanical scanning table, the microfluidic capillary was moved in the horizontal plane orthogonal to the flow direction, dragging a trapped sperm within 6.8 s from the control stream through the barrier stream into the stimulus stream. The fluorescein fluorescence, recorded synchronously to the back-reflected laser light and the bright-field images, provided a readout of the position of the trapped sperm inside the flow profile. For control experiments, the control stream with sperm, the barrier stream, and the stimulus stream consisted of HTF^{++}. To study the action of Ca^{2+}, the stimulus stream consisted of HTF^{0Ca}. To study the action of bicarbonate, the control stream with sperm consisted of bicarbonate-free HTF. For paired-plot analysis, the change in frequency was determined after reaching a stable value.

Rheotaxis assay

Human sperm in HTF^{+}, in HTF^{+} containing 100 nM progesterone, or in HTF^{+} containing 0.2% methylcellulose, or mouse sperm in TYH were observed in shallow microfluidic channels with rectangular cross section of 0.4 × 3.8 mm (Ibidi, Germany) under an inverted microscope (IX73; Olympus, Germany) equipped with a condenser (IX2-LWUCD; Olympus, Germany) and a 10× objective (UPLFLN1X2PH; Olympus, Germany). The sample was illuminated by a red LED (M660D2; Thorlabs, Germany). Images were collected at ~ 80 to ~ 125 Hz using a sCMOS camera (Zyla 4.2 Plus; Andor, UK). Sperm were exposed to a buffer flow of ~ 13.5 μl/min (human) or ~ 10 μl/min (mouse), respectively, using a syringe pump (World Precision Instruments, USA). Individual human sperm were tracked over 1.86 s in a semi-automatic fashion using a custom-made tracking tool based on the Mtrack2 plugin for ImageJ (NHI, Bethesda, USA). The angle of each track was defined by its start and end point in a two-dimensional Cartesian coordinate system with the flow direction pointing to an angle of 0° and a trajectory straight against the flow pointing to an angle of 180°. Immotile and surface-attached sperm were excluded from analysis. For each experiment, computed trajectory angles were binned into angle intervals of 90° and expressed as fractions of the sperm population (e.g., Fig 4B). Individual mouse sperm were tracked manually for 2 s; the angle of each track was defined by its start and end point in a two-dimensional Cartesian coordinate system with the flow direction pointing to an angle of 0° and a trajectory straight against the flow pointing to an angle of 180°. Like for human sperm, immotile and surface-attached sperm were excluded from analysis. For each experiment, computed trajectory angles were binned into angle intervals of 90° and expressed as fractions of the sperm population (e.g., Fig 4D).

Measurement of changes in $[Ca^{2+}]_i$

Changes in $[Ca^{2+}]_i$ were measured in sperm (in HTF^{+}) loaded with the fluorescent Ca^{2+} indicator Fluo-4-AM at 30°C in 384 multi-well plates in a fluorescence plate reader (Fluostar Omega, BMG Labtech, Ortenberg, Germany) at 30°C as described before (Schiffer *et al*, 2014; Brenker *et al*, 2018b). Briefly, sperm were loaded with Fluo-4-AM (5 μM, 20 min) at 37°C in the presence of Pluronic F-127 (0.05% w/v). After incubation, excess dye was removed by centrifugation (700 g, 5 min, room temperature). Sperm were resuspended in HTF at a density of 5×10^6 cells/ml. The wells were filled with 54 μl of the sperm suspension; fluorescence was excited at 480 nm (Fluo-4), and fluorescence emission was recorded at 520 nm. Changes in Fluo-4 fluorescence are depicted as $\Delta F/F_0$ (%), that is, the change in fluorescence (ΔF) relative to the mean basal fluorescence (F_0) before application of buffer or stimuli (6 μl).

Electrophysiology

We recorded from sperm in the whole-cell configuration as described before (Strünker *et al*, 2011). Seals between pipette and sperm were formed either at the cytoplasmic droplet or in the neck

region in standard extracellular solution (HS) containing (in mM): 135 NaCl, 5 KCl, 1 $MgSO_4$, 2 $CaCl_2$, 5 glucose, 1 Na-pyruvate, 10 lactic acid, and 20 HEPES, adjusted to pH 7.4 with NaOH. Monovalent currents were recorded in a sodium-based divalent-free solution (NaDVF) containing (in mM): 140 NaCl, 40 HEPES, and 1 EGTA, adjusted to pH 7.4 with NaOH; the pipette (10–15 MΩ) solution contained (in mM): 130 Cs-aspartate, 5 CsCl, 50 HEPES, and 5 EGTA, adjusted to pH 7.3 with CsOH. Data were not corrected for liquid junction potentials.

Immunocytochemistry

Sperm were immobilized on microscope slides and fixed for 10 min with paraformaldehyde in PBS (4%; PBS containing [in mM]: 137 NaCl, 2.7 KCl, 10 Na_2HPO_4, 1.8 KH_2PO_4, pH 7.4–7.5). To block unspecific binding sites, sperm were incubated for 1 h with blocking buffer (0.5% Triton-X 100 and 5% ChemiBLOCKER [Millipore, USA] in 0.1 M PBS, pH 7.4). Primary antibodies (anti-CatSper 4, ACC-304, Alomone Labs, Israel; polyclonal antibody raised in rabbits, directed against amino acids 384–402 of CatSper 3) were diluted in blocking buffer and incubated overnight. Fluorescent secondary antibodies were diluted in blocking buffer containing 0.5 mg/ml DAPI (Invitrogen, USA), and pictures were taken with a confocal microscope (FV1000; Olympus, Japan).

3D-STORM microscopy

Experiments were performed with a Ti-E microscope (Nikon, Japan) in an imaging buffer (50 mM Tris, pH 8, 10 mM NaCl) with an oxygen scavenging system (0.5 mg/ml glucose oxidase, 40 μg/ml catalase [Roche Applied Science, Germany or Sigma-Aldrich], and 10% [w/v] glucose), and 10 mM 2-aminoethanethiol. Images were acquired with an iXON 897 EMCCD camera (Andor, UK). 10,000–60,000 frames were acquired per data set using a 647-nm excitation laser at 100 mW at the sample plane, unless mentioned otherwise. A 405-nm laser was used to maintain an adequate number of localizations per frame. For 3D STORM acquisition, a cylindrical lens was introduced into the detection path; the "perfect focus system" (Nikon) and a vibration isolation table were used to minimize axial and lateral drifting, respectively. STORM movies were analyzed as described previously using the Nikon software package based on a technology developed by Dr. Xiaowei Zhuang (Huang *et al*, 2008). Briefly, fluorescence peaks corresponding to individual molecules were identified in each frame and fit, using least-squares fitting or maximum-likelihood estimator fitting, with a two-dimensional Gaussian to determine the (x,y) position of each molecule. For 3D imaging, the ellipticity of the Gaussian was used to assign the z coordinate. Drift correction was applied using cross-correlation. STORM images were rendered with each localization plotted as a Gaussian whose width is weighted by the inverse square root of the number of detected photons for that switching event. Images were filtered to reject molecules with emitted photon number below 500. Molecules with an aspect ratio higher than 1.5 for 2D and 2.5 for 3D datasets were rejected. Moreover, molecules that appeared for more than 10 consecutive frames were rejected. Background noise in STORM images caused by non-specifically bound antibodies, appearing as scattered localizations at low local densities, was removed by a local density filter. Low-density localizations were filtered out by removing a localization if it was surrounded by fewer than 10 localizations in the 80 nm × 80 nm region surrounding the localization.

Array CGH analysis

Patients were analyzed by array comparative genomic hybridization (CGH; Agilent platform, Agilent Technologies, Santa Clara, California, USA) using 400k arrays (#G4448A). For details, see Tüttelmann *et al* (2011).

Statistical methods

Unless otherwise indicated, data are displayed as mean ± SD.

Expanded View for this article is available online.

Acknowledgements
This work was supported by the German Research Foundation (CRU326 to T.S. and F.T.) and the Cells-in-Motion (CiM) Cluster of Excellence, Münster (FF-2016-17 to T.S. and C.F.).

Author contributions
CB, CF, and TS conceived the project. CS, SR, CB, SY, HH, DW, FT, AR, UBK, TW, AW, CK, SK, CF, and TS designed research, performed experiments, acquired, analyzed, and/or interpreted data. CS and TS wrote the manuscript. All authors revised the manuscript critically for important intellectual content and approved the manuscript.

Conflict of interest
C.B., C.S., and T.S. filed a patent entitled "Method for assessing the fertilizing potential of sperm based on longitudinal axis rotation" EP 19 191 395.3

References

Aaberg RA, Sauer MV, Sikka S, Rajfer J (1989) Effects of extracellular ionized calcium, diltiazem and cAMP on motility of human spermatozoa. *J Urol* 141: 1221 – 1224

Aitken RJ, Sutton M, Warner P, Richardson DW (1985) Relationship between the movement characteristics of human spermatozoa and their ability to penetrate cervical mucus and zona-free hamster oocytes. *J Reprod Fertil* 73: 441 – 449

Alasmari W, Barratt CL, Publicover SJ, Whalley KM, Foster E, Kay V, Martins da Silva S, Oxenham SK (2013) The clinical significance of calcium-signaling pathways mediating human sperm hyperactivation. *Hum Reprod* 28: 866 – 876

Ashkin A, Dziedzic JM, Bjorkholm JE, Chu S (1986) Observation of a single-beam gradient force optical trap for dielectric particles. *Opt Lett* 11: 288 – 290

Babcock DF, Wandernoth PM, Wennemuth G (2014) Episodic rolling and transient attachments create diversity in sperm swimming behavior. *BMC Biol* 12: 67

Baldi E, Luconi M, Muratori M, Marchiani S, Tamburrino L, Forti G (2009) Nongenomic activation of spermatozoa by steroid hormones: facts and fictions. *Mol Cell Endocrinol* 308: 39 – 46

Berger TK, Fussholler DM, Goodwin N, Bonigk W, Muller A, Dokani Khesroshahi N, Brenker C, Wachten D, Krause E, Kaupp UB *et al* (2017)

Post-translational cleavage of Hv1 in human sperm tunes pH- and voltage-dependent gating. *J Physiol* 595: 1533 – 1546

Brenker C, Goodwin N, Weyand I, Kashikar ND, Naruse M, Krahling M, Müller A, Kaupp UB, Strünker T (2012) The CatSper channel: a polymodal chemosensor in human sperm. *EMBO J* 31: 1654 – 1665

Brenker C, Rehfeld A, Schiffer C, Kierzek M, Kaupp UB, Skakkebæk NE, Strünker T (2018b) Synergistic activation of CatSper Ca^{2+} channels in human sperm by oviductal ligands and endocrine disrupting chemicals. *Hum Reprod* 33: 1915 – 1923

Brenker C, Schiffer C, Wagner IV, Tuttelmann F, Ropke A, Rennhack A, Kaupp UB, Strunker T (2018a) Action of steroids and plant triterpenoids on CatSper Ca^{2+} channels in human sperm. *Proc Natl Acad Sci USA* 115: E344 – E346

Bukatin A, Kukhtevich I, Stoop N, Dunkel J, Kantsler V (2015) Bimodal rheotactic behavior reflects flagellar beat asymmetry in human sperm cells. *Proc Natl Acad Sci USA* 112: 15904 – 15909

Carlson AE, Hille B, Babcock DF (2007) External Ca^{2+} acts upstream of adenylyl cyclase SACY in the bicarbonate signaled activation of sperm motility. *Dev Biol* 312: 183 – 192

Chung JJ, Miki K, Kim D, Shim SH, Shi HF, Hwang JY, Cai X, Iseri Y, Zhuang X, Clapham DE (2017) CatSper ζ regulates the structural continuity of sperm Ca^{2+} signaling domains and is required for normal fertility. *Elife* 6: e23082

Chung JJ, Navarro B, Krapivinsky G, Krapivinsky L, Clapham DE (2011) A novel gene required for male fertility and functional CATSPER channel formation in spermatozoa. *Nat Commun* 2: 153

Chung JJ, Shim SH, Everley RA, Gygi SP, Zhuang X, Clapham DE (2014) Structurally distinct Ca^{2+} signaling domains of sperm flagella orchestrate tyrosine phosphorylation and motility. *Cell* 157: 808 – 822

El-Sherry TM, Elsayed M, Abdelhafez HK, Abdelgawad M (2014) Characterization of rheotaxis of bull sperm using microfluidics. *Integr Biol (Camb)* 6: 1111 – 1121

Esposito G, Jaiswal BS, Xie F, Krajnc-Franken MA, Robben TJ, Strik AM, Kuil C, Philipsen RL, van Duin M, Conti M *et al* (2004) Mice deficient for soluble adenylyl cyclase are infertile because of a severe sperm-motility defect. *Proc Natl Acad Sci USA* 101: 2993 – 2998

Fechner S, Alvarez L, Bonigk W, Muller A, Berger TK, Pascal R, Trotschel C, Poetsch A, Stolting G, Siegfried KR *et al* (2015) A K(+)-selective CNG channel orchestrates Ca(2 +) signaling in zebrafish sperm. *Elife* 4: e07624

Gallagher MT, Cupples G, Ooi EH, Kirkman-Brown JC, Smith DJ (2019) Rapid sperm capture: high-throughput flagellar waveform analysis. *Hum Reprod* 34: 1173 – 1185

Harper CV, Kirkman-Brown JC, Barratt CL, Publicover SJ (2003) Encoding of progesterone stimulus intensity by intracellular $[Ca^{2+}]$ ($[Ca^{2+}]_i$) in human spermatozoa. *Biochem J* 372: 407 – 417

Hildebrand MS, Avenarius MR, Fellous M, Zhang Y, Meyer NC, Auer J, Serres C, Kahrizi K, Najmabadi H, Beckmann JS *et al* (2010) Genetic male infertility and mutation of CATSPER ion channels. *Eur J Hum Genet* 18: 1178 – 1184

Huang B, Jones SA, Brandenburg B, Zhuang X (2008) Whole-cell 3D STORM reveals interactions between cellular structures with nanometer-scale resolution. *Nat Methods* 5: 1047 – 1052

Hwang JY, Mannowetz N, Zhang Y, Everley RA, Gygi SP, Bewersdorf J, Lishko PV, Chung J-J (2019) Dual sensing of physiologic pH and calcium by EFCAB9 regulates sperm motility. *Cell* 77: 1480 – 1494

Jikeli JF, Alvarez L, Friedrich BM, Wilson LG, Pascal R, Colin R, Pichlo M, Rennhack A, Brenker C, Kaupp UB (2015) Sperm navigation along helical paths in 3D chemoattractant landscapes. *Nat Commun* 6: 7985

Jin J, Jin N, Zheng H, Ro S, Tafolla D, Sanders KM, Yan W (2007) Catsper3 and Catsper4 are essential for sperm hyperactivated motility and male fertility in the mouse. *Biol Reprod* 77: 37 – 44

Kantsler V, Dunkel J, Blayney M, Goldstein RE (2014) Rheotaxis facilitates upstream navigation of mammalian sperm cells. *Elife* 3: e02403

Kaupp UB, Solzin J, Hildebrand E, Brown JE, Helbig A, Hagen V, Beyermann M, Pampaloni F, Weyand I (2003) The signal flow and motor response controling chemotaxis of sea urchin sperm. *Nat Cell Biol* 5: 109 – 117

Kaupp UB, Strünker T (2017) Signaling in sperm: more different than similar. *Trends Cell Biol* 27: 101 – 109

Kilic F, Kashikar ND, Schmidt R, Alvarez L, Dai L, Weyand I, Wiesner B, Goodwin N, Hagen V, Kaupp UB (2009) Caged progesterone: a new tool for studying rapid nongenomic actions of progesterone. *J Am Chem Soc* 131: 4027 – 4030

Kirichok Y, Navarro B, Clapham DE (2006) Whole-cell patch-clamp measurements of spermatozoa reveal an alkaline-activated Ca^{2+} channel. *Nature* 439: 737 – 740

Lishko PV, Botchkina IL, Kirichok Y (2011) Progesterone activates the principal Ca^{2+} channel of human sperm. *Nature* 471: 387 – 391

Lishko PV, Botchkina IL, Fedorenko A, Kirichok Y (2010) Acid extrusion from human spermatozoa is mediated by flagellar voltage-gated proton channel. *Cell* 140: 327 – 337

Liu J, Xia J, Cho KH, Clapham DE, Ren D (2007) CatSperbeta, a novel transmembrane protein in the CatSper channel complex. *J Biol Chem* 282: 18945 – 18952

Loux SC, Crawford KR, Ing NH, Gonzalez-Fernandez L, Macias-Garcia B, Love CC, Varner DD, Velez IC, Choi YH, Hinrichs K (2013) CatSper and the relationship of hyperactivated motility to intracellular calcium and pH kinetics in equine sperm. *Biol Reprod* 89: 123

Mannowetz N, Miller MR, Lishko PV (2017) Regulation of the sperm calcium channel CatSper by endogenous steroids and plant triterpenoids. *Proc Natl Acad Sci USA* 114: 5743 – 5748

Miki K, Clapham DE (2013) Rheotaxis guides mammalian sperm. *Curr Biol* 23: 443 – 452

Miller MR, Kenny SJ, Mannowetz N, Mansell SA, Wojcik M, Mendoza S, Zucker RS, Xu K, Lishko PV (2018) Asymmetrically positioned flagellar control units regulate human sperm rotation. *Cell Rep* 24: 2606 – 2613

Miller MR, Mannowetz N, Iavarone AT, Safavi R, Gracheva EO, Smith JF, Hill RZ, Bautista DM, Kirichok Y, Lishko PV (2016) Unconventional endocannabinoid signaling governs sperm activation via sex hormone progesterone. *Science* 352: 555 – 559

Muschol M, Wenders C, Wennemuth G (2018) Four-dimensional analysis by high-speed holographic imaging reveals a chiral memory of sperm flagella. *PLoS ONE* 13: e0199678

Navarro B, Kirichok Y, Chung JJ, Clapham DE (2008) Ion channels that control fertility in mammalian spermatozoa. *Int J Dev Biol* 52: 607 – 613

Nosrati R, Driouchi A, Yip CM, Sinton D (2015) Two-dimensional slither swimming of sperm within a micrometre of a surface. *Nat Commun* 6: 8703

Oren-Benaroya R, Orvieto R, Gakamsky A, Pinchasov M, Eisenbach M (2008) The sperm chemoattractant secreted from human cumulus cells is progesterone. *Hum Reprod* 23: 2339 – 2345

Publicover SJ, Giojalas LC, Teves ME, de Oliveira GS, Garcia AA, Barratt CL, Harper CV (2008) Ca^{2+} signaling in the control of motility and guidance in mammalian sperm. *Front Biosci* 13: 5623 – 5637

Quill TA, Ren D, Clapham DE, Garbers DL (2001) A voltage-gated ion channel expressed specifically in spermatozoa. *Proc Natl Acad Sci USA* 98: 12527 – 12531

R, Thyberg P (1984) Rotational and translational swimming of human spermatozoa: a dynamic laser light scattering study. *Cytometry* 5: 327 – 332

Ren D, Navarro B, Perez G, Jackson AC, Hsu S, Shi Q, Tilly JL, Clapham DE (2001) A sperm ion channel required for sperm motility and male fertility. *Nature* 413: 603 – 609

Rennhack A, Schiffer C, Brenker C, Fridman D, Nitao ET, Cheng YM, Tamburrino L, Balbach M, Stolting G, Berger TK *et al* (2018) A novel cross-species inhibitor to study the function of CatSper Ca^{2+} channels in sperm. *Br J Pharmacol* 175: 3144 – 3161

Schaefer M, Hofmann T, Schultz G, Gudermann T (1998) A new prostaglandin E receptor mediates calcium influx and acrosome reaction in human spermatozoa. *Proc Natl Acad Sci USA* 95: 3008 – 3013

Schiffer C, Müller A, Egeberg DL, Alvarez L, Brenker C, Rehfeld A, Frederiksen H, Waschle B, Kaupp UB, Balbach M *et al* (2014) Direct action of endocrine disrupting chemicals on human sperm. *EMBO Rep* 15: 758 – 765

Seifert R, Flick M, Bonigk W, Alvarez L, Trotschel C, Poetsch A, Muller A, Goodwin N, Pelzer P, Kashikar ND *et al* (2015) The CatSper channel controls chemosensation in sea urchin sperm. *EMBO J* 34: 379 – 392

Smith JF, Syritsyna O, Fellous M, Serres C, Mannowetz N, Kirichok Y, Lishko PV (2013) Disruption of the principal, progesterone-activated sperm Ca^{2+} channel in a CatSper2-deficient infertile patient. *Proc Natl Acad Sci USA* 110: 6823 – 6828

Strünker T, Goodwin N, Brenker C, Kashikar ND, Weyand I, Seifert R, Kaupp UB (2011) The CatSper channel mediates progesterone-induced Ca^{2+} influx in human sperm. *Nature* 471: 382 – 386

Tamburrino L, Marchiani S, Minetti F, Forti G, Muratori M, Baldi E (2014) The CatSper calcium channel in human sperm: relation with motility and involvement in progesterone-induced acrosome reaction. *Hum Reprod* 29: 418 – 428

Tamburrino L, Marchiani S, Vicini E, Muciaccia B, Cambi M, Pellegrini S, Forti G, Muratori M, Baldi E (2015) Quantification of CatSper1 expression in human spermatozoa and relation to functional parameters. *Hum Reprod* 30: 1532 – 1544

Torres-Flores V, Picazo-Juárez G, Hernández-Rueda Y, Darszon A, González-Martínez MT (2011) Sodium influx induced by external calcium chelation decreases human sperm motility. *Hum Reprod* 26: 2626 – 2635

Tresguerres M, Levin LR, Buck J (2011) Intracellular cAMP signaling by soluble adenylyl cyclase. *Kidney Int* 79: 1277 – 1288

Tung CK, Ardon F, Fiore AG, Suarez SS, Wu M (2014) Cooperative roles of biological flow and surface topography in guiding sperm migration revealed by a microfluidic model. *Lab Chip* 14: 1348 – 1356

Tung CK, Ardon F, Roy A, Koch DL, Suarez SS, Wu M (2015) Emergence of upstream swimming via a hydrodynamic transition. *Phys Rev Lett* 114: 108102

Tüttelmann F, Simoni M, Kliesch S, Ledig S, Dworniczak B, Wieacker P, Röpke A (2011) Copy number variants in patients with severe oligozoospermia and Sertoli-cell-only syndrome. *PLoS ONE* 6: e19426

Wang H, Liu J, Cho KH, Ren D (2009) A novel, single, transmembrane protein CATSPERG is associated with CATSPER1 channel protein. *Biol Reprod* 81: 539 – 544

Xie F, Garcia MA, Carlson AE, Schuh SM, Babcock DF, Jaiswal BS, Gossen JA, Esposito G, van Duin M, Conti M (2006) Soluble adenylyl cyclase (sAC) is indispensable for sperm function and fertilization. *Dev Biol* 296: 353 – 362

Zhang Y, Malekpour M, Al-Madani N, Kahrizi K, Zanganeh M, Lohr NJ, Mohseni M, Mojahedi F, Daneshi A, Najmabadi H *et al* (2007) Sensorineural deafness and male infertility: a contiguous gene deletion syndrome. *J Med Genet* 44: 233 – 240

Zhang Z, Liu J, Meriano J, Ru C, Xie S, Luo J, Sun Y (2016) Human sperm rheotaxis: a passive physical process. *Sci Rep* 6: 23553